OE Optical Engineering

RESEARCH PAPER

Lensless projection of automotive light distributions using an advanced printer for volume holographic optical elements

Lukas T. Hiller[a,b,*] **and Jörg Wallaschek**[a]

[a]Leibniz University Hanover, Institute of Dynamics and Vibration Research, Garbsen, Germany
[b]HELLA GmbH & Co. KGaA, L-LAB, Lippstadt, Germany

ABSTRACT. Volume holographic optical elements (vHOEs) are currently used in various applications, such as augmented reality displays or wearables. Yet, the use of vHOEs as illumination optics has not found its way into products. In automotive exterior lighting, vHOEs could enable unique styling, reduction of installation space, weight, and material. However, in headlamps, rear lamps, or signal lamps, several technical and conceptional challenges must be addressed. One of these challenges is to replace lasers, which are expensive and have high safety demands, by light emitting diodes (LEDs), which are widely used in the field of automotive lighting. The reconstruction of volume holograms with LEDs is straightforward for graphical holograms showing a three-dimensional scene. For automotive exterior lighting, however, the hologram is not just a design element, but in addition must feature a light distribution fulfilling all the legal requirements. The vHOE thus becomes the most important functional element of the lighting system projecting the light distribution without an additional lens. For instance, the low beam distribution must provide a sharp, asymmetric cutoff line and white color, which turns out to be difficult. We have developed an improved manufacturing technique of such vHOEs, using two spatial light modulators. We present the design, the holographic printer setup, and first experimental results of vHOE samples.

Keywords: hologram printer; holographic optical element; automotive lighting; light emitting diode; lensless projection

Paper 20240110SS received Jan. 30, 2024; revised Apr. 23, 2024; accepted May 22, 2024; published Jun. 14, 2024.

1 Introduction

Holography has evolved into a wide and versatile research and commercial field since the principle was shown by Gabor et al.[1] Early work of Leith and Upatnieks showed the potential of holograms for the use as holographic optical elements (HOEs),[2] and today new photopolymer-based hologram recording materials enable precise volume HOEs (vHOEs).[3] Designing vHOEs for white light and divergent illumination, as emitted by light emitting diodes (LEDs), has proven difficult due to the wavelength and angular selectivity of volume holograms, as analyzed by Kogelnik.[4–9] To overcome the limitations of simple one step recording setups, hologram printers are used for the exposure of master holograms. The goal is to manufacture either large scale diffractive optics[10] or HOEs for complex reconstruction wave fronts, where angles of incidence must be compensated during manufacturing.[11,12] Those printers have in common that the

*Address all correspondence to Lukas T. Hiller, lukas.hiller@l-lab.de

hologram is divided into a set of hogels or subholograms, which are exposed sequentially. Here, the respective subholograms can be designed for different optical purposes.

Today, vHOEs are not used for exterior automotive lighting. The task of reshaping the light of a source into a target light distribution with a vHOE in an efficient way poses challenges for researchers and creates the need for new exposure techniques in hologram printers.[13] Our goal is to use vHOEs as the main and crucial optical element in automotive main lighting. In headlamps, rear combination lamps (RCLs) and signal functions, there are several advantages of photopolymer based holograms. In the design and cost optimization driven automotive industry, holograms are technology enablers for lightweight, compact, and simple lighting units while providing unique styling features, such as transparent optical elements or the black panel effect (light out of nowhere). To do so, the vHOE concept of Giehl et al.[9] is adapted and further developed.

2 vHOES for LED Illumination

It seems to be contradictory to use a strictly angular and wavelength selective vHOE for the generation of white light distribution with a divergent light source. However, with the right concept, there is a possibility to overcome the issues and benefit from the properties of volume holograms.

2.1 Adaptation to Divergence

Giehl et al. showed that the divergence of an LED can be taken into account when manufacturing the vHOE.[9] Here, so called volume holographic cell arrays (VCAs) are used, where the hologram is divided into an array of subholograms. During exposure, the reference beam angle is adapted for each subhologram. The respective reference beam angles recreate the illumination angles of an LED. By choosing a small subhologram size of $0.7\ \text{mm} \times 0.7\ \text{mm}$, a good approximation of the LEDs radiation characteristics can be achieved over a wide angular range with altitude $\theta(\text{deg}) \in [5, 70]$ and azimuth $\phi(\text{deg}) \in [5, 175]$. However, within one subhologram, the wavefront is considered as a plane wave.

Another approach by Karthaus et al. uses the complex conjugated phase of a local LED wavefront and a spatial light modulators (SLMs) to adapt the vHOE for LED illumination in Ref. 7. Different wavefront approximations were tested and compared. The best reconstruction was achieved with a measured wavefront of the used LED. Nevertheless, a spherical approximation showed good results as well. Unfortunately, this approach is limited to a small angular range of ± 2 deg limited by the SLM and the wavefront measurements.

In the vHOE concept of this contribution, both approaches by Giehl et al. and Karthaus et al. are combined to enable a wide angular range with precise local adaptation to the LED illumination. As shown in Fig. 1(a), the VCA concept is used for the global angle of incidence adaptation, and each subhologram is optimized for the respective mean angle of incidence.

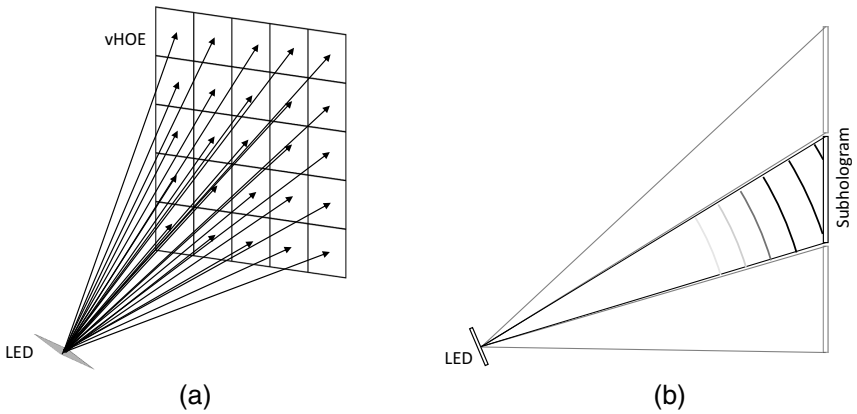

Fig. 1 Concept for the adaptation of the hologram to divergent LED illumination. With (a) global angle of incidence adaptation and (b) local wavefront approximation.

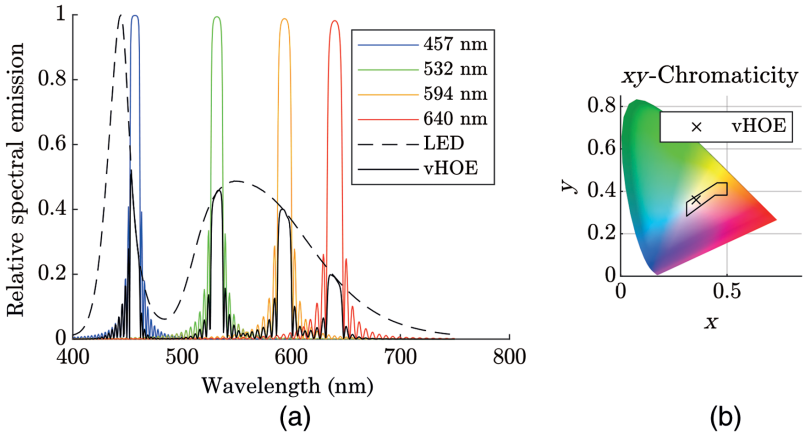

Fig. 2 Wavelength selection for the vHOE exposure to achieve a white light distribution with LED reconstruction with (a) spectra and (b) chromaticity.

In addition, the LED illumination is approximated in each subhologram with a spherical wavefront like in Fig. 1(b). The local wavefront approximation is realized by an additional SLM in the hologram printer.

2.2 Wavelengths

The second issue of vHOEs for LED illumination is the wavelength selectivity. In an earlier contribution,[14] we calculated the chromaticity of vHOEs for the illumination of different LEDs using the coupled wave theory (CWT) by Kogelnik.[4] With four exposure wavelengths of 457, 532, 594, and 640 nm and LED reconstruction, a white light distribution can be generated fulfilling the united nations economic commission for Europe (ECE) regulations for the color locus of white light in main light functions of motorized vehicles.[15] Figure 2 shows the results of a CWT simulation for an automotive phosphor converted white light LED.

In Fig. 2(a), the relative spectral emission of an automotive phosphor converted white light LED is displayed. For each exposure wavelength, the vHOE has an associated spectral selectivity. The spectrum of the reconstructed light distribution is determined by the vHOEs spectral selectivity and the LED spectrum. The resulting spectrum is then evaluated regarding the color locus in Fig. 2(b). The material parameters are set to a refractive index modulation of $\Delta n = 0.044$ and a thickness of $d = 40\,\mu$m of the photopolymer. For the first evaluation, the refractive index of the photopolymer is set to $n = 1$ and it is assumed that there is no attenuation by absorption. Using this configuration, we find that the color locus is within the boundaries of the ECE regulations. Therefore, the wavelengths are suitable for the exposure of vHOEs for automotive use cases.

2.3 Light Distribution

Until this point, the adaptation of the vHOE to divergent illumination and the spectral selectivity was considered. Generating the actual light distribution, however, is another challenge. Automotive light distributions differ greatly depending on their function. While signal functions, such as break lights and turn indicators, are monochromatic and blurred, the low beam distribution has a sharp cutoff line with high contrast and needs white light.[15] Generating a sharp cutoff line with a vHOE and LED illumination is challenging. The light distribution generated by a vHOE is determined by the object wave in the hologram recording process. Hence, the laser radiation must be modulated to form the required object wave. Our printer uses a phase only SLM. Consequently, the task is to find a phase profile for the SLM to generate the desired light distribution in the far field. This is the typical task of computer generated holograms (CGHs). Different algorithms, such as the Gerchnberg–Saxton error reduction algorithm (GS)[16] and its variants, for example, in Ref. 17, have been developed. For the reconstruction with an incoherent LED, however, the suitability of different approaches and algorithms must be investigated.

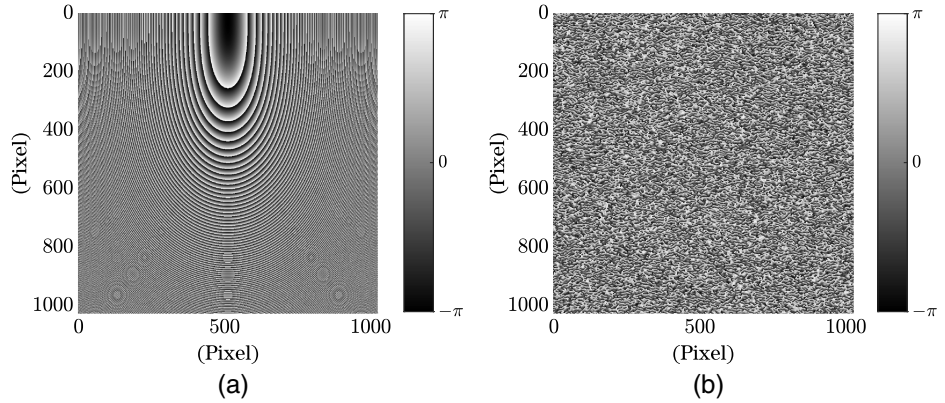

Fig. 3 Comparison of smooth (a) and GS (b) phase distribution. (a) Smooth phase distribution of CGH for a low beam distribution with flat cutoff line. (b) GS calculated phase distribution of CGH for a low beam distribution with random initial phase.

Due to the lack of spatial coherence of LEDs, we assume that standard algorithms, such as the GS, using a randomized start phase are not suitable for LED reconstruction. Therefore, we developed an algorithm to convert automotive free-form reflectors into CGHs.[18] The crucial difference of the CGH calculated by GS and our algorithm is the resulting phase profile of the CGH. While the GS delivers a CGH with a rapidly changing phase profile our algorithm results in a smoother phase profile. An example for a CGH calculated by our algorithm is shown in Fig. 3(a) and a CGH calculated by GS with random initial phase in Fig. 3(b). A low beam distribution is realized with a flat cutoff line. The performance of different algorithms will be investigated in another contribution.

We defined the adaptation to divergent light sources with the reference wave, the required wavelengths, and the object wave encoding the light distribution of the vHOEs for automotive lighting purposes. The manufacturing of such vHOEs requires an advanced hologram printer and new exposure techniques. There are several technical challenges to overcome.

3 Hologram Printer

This section describes the working principle of the hologram printer to manufacture the previously described vHOEs for LED illumination and automotive light distributions. This printer further develops the idea of Giehl[12] and uses the results of investigations from Karthaus.[7] Using two phase, only SLMs was mentioned by Hofmann et al. in Ref. 11. However, with SLMs only small deviations in the illumination angle can be compensated. Our printer synthesizes complex wavefronts and illumination setups over a large angular range with the altitude $\theta(\text{deg}) \in [10, 70]$ and the azimuth $\phi(\text{deg}) \in [10, 170]$. Figure 4 shows a sketch of the hologram printer and its key components.

Our hologram printer uses four laser sources ($L_1 - L_4$), an acousto-optic tunable filter (AOTF), two phase only SLMs, two motorized rotation stages with a $\lambda/2$ waveplate, and a polarization filter, five motorized linear stages for beam path adjustments, a two-dimensional translation stage for substrate positioning, and a large parabolic mirror. First, the laser sources and their modulation are described. Then, the optical setup is explained, some beam corrections that must be taken into account are derived and their technical implementations are developed.

3.1 Laser Sources and Wavelength Selection

Suitable laser sources are the key to successful holography. There is a need for single frequency continuous wave lasers with long temporal coherence lengths, good wavelength stability, and high quality beam profiles.[19] In addition, one must chose the correct wavelengths to achieve a white light reconstruction of the vHOE with LED illumination. As mentioned earlier, we found that four wavelengths are suitable for our application. A blue (457 nm), a green (532 nm), a yellow (594 nm), and a red (640 nm) laser are brought on the same optical axis in a laser combiner housing with dichroic mirrors. The lasers must run continuously and at hundred percent of

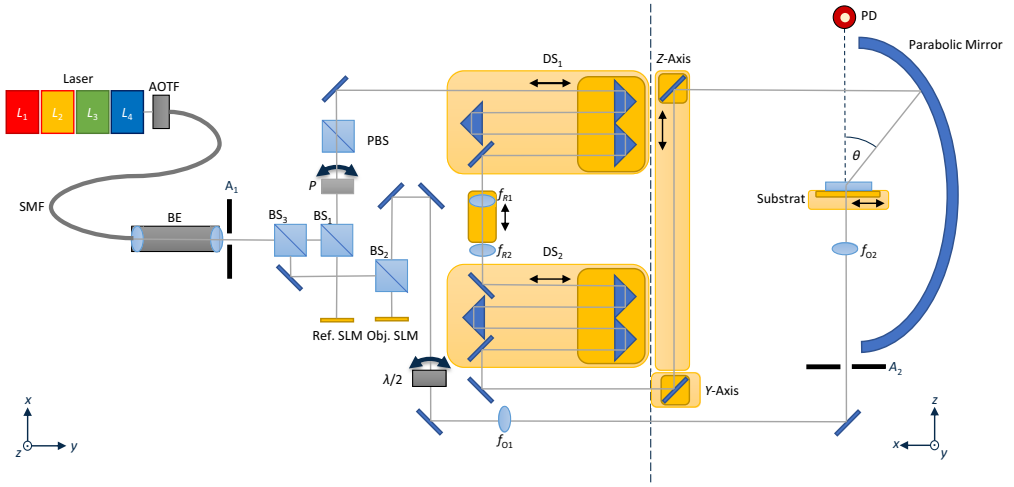

Fig. 4 Sketch of the hologram printer setup. With laser sources L_{1-4}, acousto-optic tunable filter AOTF, beam expander BE, aperture masks $A_{1,2}$, beam splitters BS_{1-3}, polarizing beam splitter PBS, spatial light modulators $SLM_{Ref,Obj}$, linear polarization filter P, waveplate $\lambda/2$, delay stages $DS_{1,2}$, lenses $f_{R1,R2,O1,O2}$ and photo diode PD.

their power to ensure optimal beam quality. On the contrary, the respective lasers highly differ in their output power, must be blocked between single exposures, and the power output must be modulated individually per wavelength. An AOTF with a multi-channel driver is the solution to these issues but brings new challenges. Although, the combiner housing enables very good overlap of the respective laser beams, after passing the AOTF the beams show dispersion, regardless of the alignment effort. Following this, the overlap of the laser beams is not guaranteed for the long optical path lengths in the printer setup. Therefore, our solution is to use a broadband single mode optical fiber with polarization preservation to ensure perfect overlap. After passing the AOTF, the laser beams are coupled into the single mode fiber. The light is guided in the fiber and only one transversal mode is possible resulting in a perfect overlap of the Gaussian beam profiles of the respective wavelengths at the fibers output. Here, the deviation of the optimal coupling direction only causes attenuation of the laser power.[20] This setup enables arbitrary wavelength mixture compositions while preserving the overlap and beam properties.

3.2 Optical Setup

After the wavelength selection and power modulation by the AOTF, the laser light is delivered by a single mode optical fiber to the printer setup. A beam expander with a fixed magnification of 20 is used to enlarge the collimated laser beam. An aperture mask A_1 is used to shape the beam profile into a square of 7 mm × 7 mm according to the active area of the SLMs. The beam is then divided into the reference and object beam using a beam splitter BS_3. In addition, two beam splitters BS_1 and BS_2 are used to illuminate the respective SLMs and to ensure that there is no coupling from the reference beam to the object beam and vice versa. The respective beam paths are in $4f$ configuration to ensure a beam diameter reduction of the factor 10. The respective SLMs are imaged into the substrate plane and superimposed for interferometric recording of the vHOE. As shown in Fig. 4, the printer is suited for recording reflection, when object and reference wave are entering the substrate plane from opposite sides, and transmission type vHOEs, when object and reference wave entering from the same side. However, we will focus on reflection holograms only. The authors chose two identical phase only SLMs (*HOLOEYE LETO 2*) with a native resolution of 1920 × 1080. With the aperture mask A_1, the active areas of the SLMs are reduced to ∼1024 × 1024 pixels. These SLMs exhibit a pixel pitch of 6.4 μm and are configured with a voltage lookup table optimized to achieve a maximum 2π phase shift for 633 nm wavelengths. The gray values sent to the SLMs, corresponding to specific phase shifts, are recalibrated for the respective wavelengths.

3.2.1 *Object beam*

The object beam provides the information about the desired light distribution that should be encoded into the vHOE. To shape the parallel light of the laser source into the light distribution, a phase only SLM is used with a suitable phase profile of the CGH. The $4f$ objective lens system is realized by two achromatic lenses with $f_{O1} = 750$ mm and $f_{O2} = 75$ mm. The reduction of the SLM image also increases the divergence. Therefore, light distributions with: ± 10 deg opening angle can be realized. Furthermore, the object beam path features an achromatic $\lambda/2$ waveplate mounted to a motorized rotation stage. This enables to match the polarization of the reference and object waves in the substrate plane. A more detailed explanation is given in Sec. 3.3.

3.2.2 *Reference beam*

To expose vHOEs for divergent reconstruction light sources, a complex synthesis of the reference wave is required. Since large divergence angles are not possible with SLMs, we use a hybrid approach with a parabolic mirror for global angle adjustment and a phase only SLM for local wavefront adaptation. A parabolic mirror has the property of a fixed focal point for light rays entering the mirror parallel to its axis of symmetry. We use this property to change the angle of incidence of the reference wave to the substrate plane. Two perpendicular mounted motorized linear axes (X and Z) are used to adjust the position of the reference wave on the parabolic mirror. By entering from different points, the focal point stays fixed but the angle of incidence changes. While the focal point does not change, the focal length differs greatly, creating two major challenges. First, the optical path length must be adjusted, and second there is a need for an adaptive lens system to ensure the $4f$ condition for each reference angle. Figure 5 shows the effective focal length of the parabolic mirror f_{eff} in respect to the angles of incidence on the substrate plane, the altitude θ, and the azimuth ϕ.

As shown in Fig. 5, f_{eff} varies from 160 to 350 mm. To achieve a beam reduction of the factor 10, the $4f$ configuration is realized by optical delay stages DS1 and DS2 and an adaptive lens system f_{Sys}. The lenses $f_{R1} = -200$ mm and $f_{R2} = 200$ mm are positioned by a motorized linear axis in a distance up to 50 mm enabling an effective focal length of $f_{\text{Sys}}(\text{mm}) \in [673, 4245]$. The $4f$ configuration is fulfilled if $f_{\text{sys}} = 10 \cdot f_{\text{eff}}$ and the path lengths are adapted accordingly. All the required axis positions are calculated by the matrix formalism for the respective reference angles θ and ϕ. Furthermore, the reference beam features a linear polarization filter mounted to a motorized rotation axis and a polarizing beam splitter PBS. This configuration delivers an additional power modulation of the reference beam.

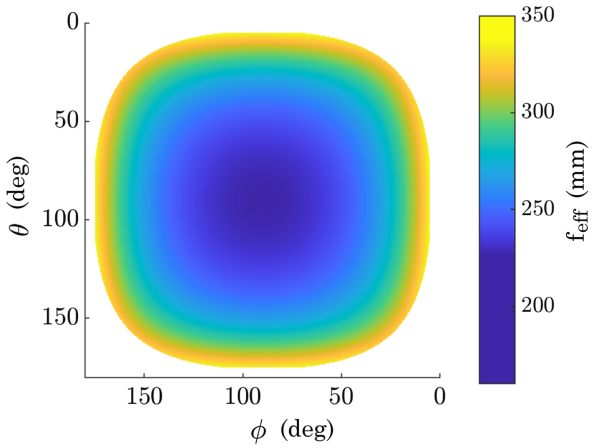

Fig. 5 Effective focal length of the parabolic mirror for the reference angles altitude θ and azimuth ϕ.

3.3 Beam Corrections

So far, the printer realizes an interferometric recording of two individually phase modulated waves and the variation of the reference angle. However, there are several beam corrections that must be implemented before writing efficient vHOEs. For a good contrast of the interference pattern, the power ratio of the respective beams must be matched inside the hologram recording material. Furthermore, the polarization must be aligned accordingly.[21]

3.3.1 *Polarization*

By changing the angle of incidence of the reference beam with the parabolic mirror, the polarization rotates as well in respect to the polarization of the object beam. For good contrast of the interference pattern and therefore good efficiency of the vHOE, an aligned polarization is required. Furthermore, *s*-polarization is required such that the electric field vectors of the object and reference wave are coincident in the substrate plane. The polarization is matched by rotating the linear polarization of the object beam with a $\lambda/2$-waveplate mounted to a motorized rotation axis. The required angle of rotation is calculated as described by Giehl et al. in Ref. 12.

3.3.2 *Beam ratio*

The adaptation of the reference and object beam ratio is realized by attenuation of the reference beam power. The beam splitter BS_3 is used to divide the laser beam in the respective beam paths. A splitting ratio of 70% transmission and 30% reflection is used to provide more power in the reference beam. The higher power is needed for two reasons. First, the reference beam features a longer optical beam path with more optical components in comparison to the object beam path. Second, the reference beam changes its angle of incidence ψ in respect to the holographic film, where ψ is the effective angle of incidence given by θ and ϕ. Here, Fresnel reflection occurs, which must be compensated to provide a beam ratio of 1:1 inside the holographic recording medium. As shown in Fig. 6(b), the transmission changes with the angle of incidence. As mentioned, in our setup *s*-polarization is used.

In Fig. 6(a), the optical power of the reference beam P_{Ref} is measured in the substrate plane for different rotation angles of the linear polarization filter P for the respective laser wavelengths, which are modulated to 10 mW each at the optical fiber exit. The power was measured for $\alpha_P(\mathrm{deg}) \in [5, 65]$ in steps of 5 deg. The data are fit to the function Eq. (1), where $P_{\mathrm{Ref},\lambda,\mathrm{max}} = P_{\mathrm{Ref},\lambda}(\alpha = 0\ \mathrm{deg})$ is the power at the substrate plane with no attenuation by the linear polarization filter P and b, c are fitting constants. The optimal beam ratio inside in recording material is given by Eq. (2). Inserting Eq. (1) into Eq. (2) and solving after α delivers Eq. (4):

$$P_{\mathrm{Ref},\lambda}(\alpha) = \frac{P_{\mathrm{Ref},\lambda,\mathrm{max}}(\cos(b \cdot \alpha + c) + 1)}{2}, \tag{1}$$

$$T_{s,\mathrm{Obj}} \cdot P_{\mathrm{Obj}} = T_{s,\mathrm{Ref}}(\psi) \cdot P_{\mathrm{Ref},\lambda}(\alpha), \tag{2}$$

$$\mathrm{BR}' = \frac{2 \cdot T_{s,\mathrm{Obj}} \cdot P_{\mathrm{Obj}}}{P_{\mathrm{Ref},\lambda,\mathrm{max}} \cdot T_{s,\mathrm{Ref}}(\psi)} - 1 \tag{3}$$

$$\alpha_P(\psi) = \frac{\arccos(\mathrm{BR}') - c}{b}. \tag{4}$$

Equation (4) provides the required rotation angle of the linear polarization filter $\alpha_P(\psi)$ for the reference beam angle of incidence ψ for the respective laser wavelength λ. The transmission of the object beam $T_{s,\mathrm{Obj}}$ is assumed to be 95%. The resulting curves for $\alpha_P(\psi)$ are displayed in Fig. 6(c). Angles of incidence up to 85 deg can be compensated for 457, 532, and 640 nm. For 594 nm, a maximum of 80 deg can be matched. However, the printer only uses a maximum of 70 deg. The wavelength dependency follows from the chromatic effects of the optical components in the setup and the varying diffraction efficiencies of the SLMs.

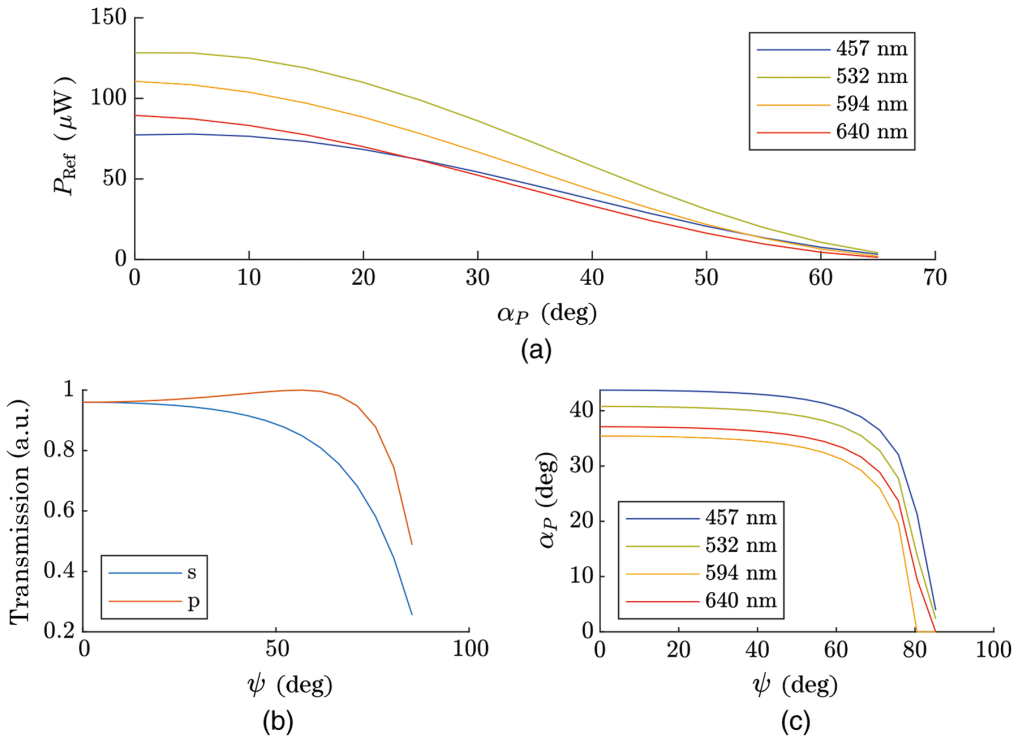

Fig. 6 Beam power ratio adjustment of reference and object beam. (a) Power P_{Ref} at the substrate plane in respect to the rotation angle α_P of the linear polarization filter of the reference beam path. (b) Fresnel transmission for *s*- and *p*-polarized light for the reference beam angle ψ. (c) Required rotation α_P of the linear polarization filter for the respective reference beam angle ψ.

4 Results

Now that the hologram printer is described, suitable exposure parameters must be found, the beam correction mechanisms must be tested, and the performance of the vHOEs is to be investigated. First, different exposure parameters are examined in Sec. 4.1. The next step is to evaluate the performance of the LED wavefront approximation in Sec. 4.2. Finally, a vHOE for a miniaturized stoplight function is investigated in Sec. 4.3.

4.1 Parameters

For the exposure parameters, the exposure dose is of high interest. The task is to maximize the diffraction efficiency of the subholograms for the respective laser wavelength. For this purpose, slanted diffraction gratings are recorded by superimposing two plane waves. Then, holograms with different exposure times are recorded. After recording, the holograms are flood cured with a spectral lamp for 45 m. To evaluate the efficiency a photo diode (PD) is mounted in the hologram printer (Fig. 4) in a distance of 50 cm to the substrate plane. This offers the possibility to measure the power of the reconstructed object beam for each subhologram separately. The measured power $P_{\lambda,k,i,j}$ is recorded into a file and then divided by the reference beam power $P_{\mathrm{Ref},\lambda}(\alpha)$ known from the beam corrections described in Sec. 2 to determine the diffraction efficiency $\eta_{k,i,j}$. Here, k is the hologram with certain exposure properties and i, j encodes the specific subhologram Eq. (5). The diffraction efficiency of each hologram is then determined by Eq. (6):

$$\eta_{k,i,j} = \frac{P_{\lambda,k,i,j}}{P_{\mathrm{Ref},\lambda}(\alpha)}, \tag{5}$$

$$\eta_k = \frac{\sum_{i,j} \eta_{k,i,j}}{i \cdot j}. \tag{6}$$

4.1.1 *Exposure time*

In the first step, the reference angle is fixed at $\phi = 25$ deg and $\phi = 90$ deg and the object beam is coincident with the substrate normal. Note that the reference beam angles θ and ϕ are defined in the coordinate system of the parabolic mirror as shown in Fig. 5. Here, $\phi = 90$ deg is the central axis of the parabolic mirror. The BAYFOL HX 200 (COVESTRO) recording material is used. Per wavelength nine test holograms of the size $8 \times 8 = 64$ subholograms are manufactured for different exposure times. These test holograms are recorded into one sample and arranged in a matrix pattern of 3×3 with a distance of 5 mm. In between the exposure of each hologram, a break of 60 s was implemented to avoid crosstalk effects. In Ref. 22, reaction diffusion models of the photopolymer are discussed. However, the break is chosen much longer to avoid any effects by oxygen inhibition. The subholograms are recorded sequentially in an *s*-pattern without any break time except the time to move the axes of the printer. The laser power is fixed at 10 mW for each laser wavelength, measured at the single mode fiber SMF exit. The results are shown in Fig. 7.

For each test hologram in Fig. 7, there are 64 subholograms and measurements. This allows statistical analysis of the behavior of the subholograms for different exposure times. There is a general increase of the median efficiency with longer exposure times until a certain threshold is reached. This is to be expected and mentioned in other investigations (e.g., Ref. 22). However, after the threshold is reached, there is a decreased median efficiency and a higher variance of the measured efficiencies. Furthermore, the count of outliers increases. Obviously, different second order effects decrease the efficiency. For example, the subholograms are positioned close to each other with an offset of $d = 0.15$ mm for a subhologram size of 0.7 mm $\times$ 0.7 mm. For longer exposure times, the photochemical reaction in the recording medium eventually diffuses into the

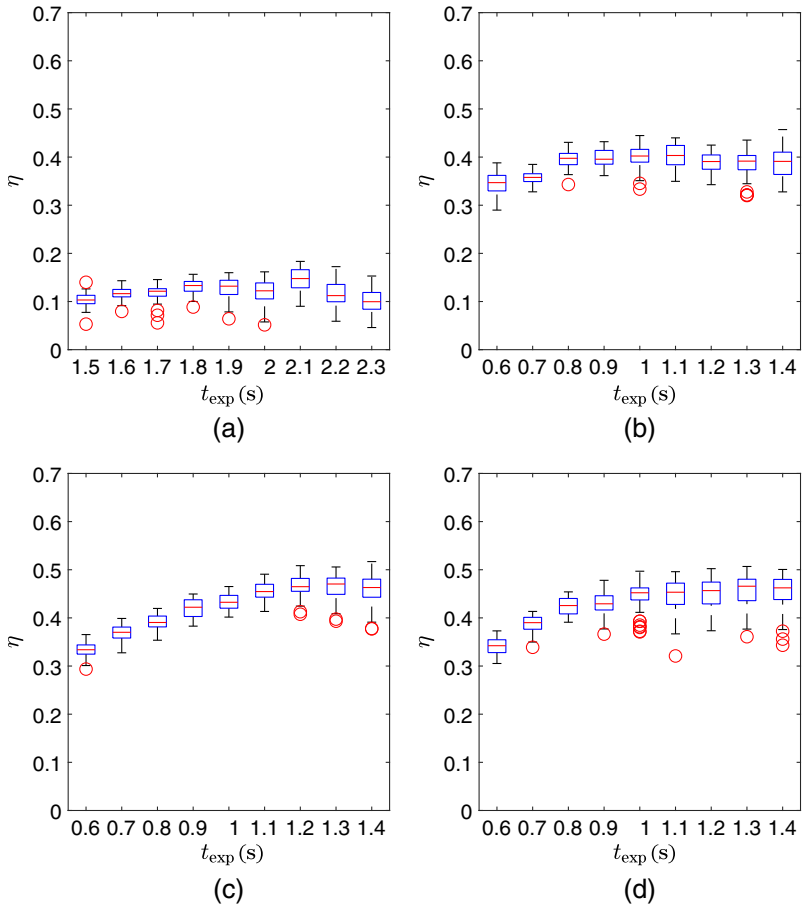

Fig. 7 Efficiency η box plots of test holograms for the respective wavelengths λ and exposure times t_{exp}. The laser power is set to 10 mW for each laser source. The red circles indicate outliers. (a) 457 nm, (b) 532 nm, (c) 594 nm, and (d) 640 nm.

recording area of adjacent subholograms reducing the reachable refractive index modulation. The smaller the variance of the subholograms efficiencies, the better the reproducibility of the measurements. Note that the outliers are always of lower efficiency than the lower adjacent, but never higher than the upper adjacent. This indicates that outliers belong to defective subholograms.

The maximum efficiency is lower than expected. Comparing the experimental results with simulations from the CWT, only <50% diffraction efficiency is achieved instead of >90%. In particular, the efficiency of the holograms recorded with 457 nm is below 20% and differs largely from the simulation results. There might be some manufacturing effects that decrease the efficiency. The recording medium shrinks in thickness and changes its refractive index when it is flood cured. This causes a shrinkage of the holographic grating and following the optimal reference beam angle for reconstruction changes compared to the recording reference angle. However, in our measurements, we use the same reference beam angle for the reconstruction and recording. This results in a decreased diffraction efficiency. Furthermore, the SLMs use an optimized voltage profile for 2π phase modulation at 633 nm with an 8-bit modulation depth. For shorter wavelengths, however, the modulation depth is decreased to ensure 2π modulation. This may cause a deviation from a sinusoidal diffraction index modulation in the recording medium and a decrease in efficiency. In addition, it must be noted that the parabolic mirror used in the reference beam path decreases the imaging quality due to imperfections of the surface. There might be a chromatic dependency if the aluminum grain size of the parabolic mirror is in the order of the respective laser wavelength. Finally, the used recording material features residual absorption after the flood cure. The absorption is higher for shorter wavelengths, decreasing the efficiency for the 457 nm holograms.

4.1.2 *Reference beam angle*

The beam corrections of Sec. 3.3 are mainly required for the adaptation of the reference beam angle of incidence ψ on the substrate. The goal is to correct the polarization and the beam ratio inside the recording medium for an optimized contrast of the interference pattern and following a high diffraction efficiency. A metric to evaluate this correction effort is the reproducibility of the diffraction efficiency for different reference beam angles. Therefore, a set of test holograms is recorded for different reference beam angles ψ using the optimized exposure time. In this investigation, only θ is varied. The holograms are patterned analogous to the previous exposure time test holograms and without loss of generality the recording wavelength of $\lambda = 640$ nm is chosen. This wavelength with exposure time of $t_{\text{exp}} = 1.2$ s delivered the best results in the previous investigations.

Figure 8 shows the respective efficiencies for different reference beam angles and compares the implemented beam ratio correction with a constant beam ratio. For the constant case, the

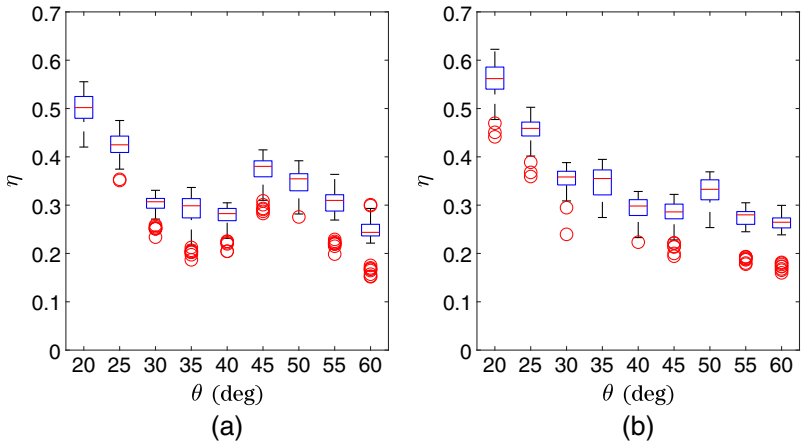

Fig. 8 Efficiency η box plots of test holograms for different reference beam angles θ. The wavelength $\lambda = 640$ nm is used and an exposure time is set to $t_{\text{exp}} = 1.2$ s. The laser power is set to 10 mW. The red circles indicate outliers (a) with and (b) without beam ratio correction.

rotation angle of the linear polarization filter is set to $\alpha = 0$. In Fig. 8(a), the efficiency is expected to be constant. Unfortunately, the measured data prove different. The variation of the diffraction efficiency changes largely with the reference beam angle θ. Without the corrections displayed in Fig. 8(b), the efficiency decreases for higher angles due to Fresnel reflection. While the corrected ratio shows high efficiencies $\eta > 40\%$ for $\theta \leq 25$ deg, in the interval $30 \leq \deg\theta \leq 40$ deg the efficiency is decreased to $\eta \approx 30\%$ and then increases again for $\theta \geq 45$ deg. Therefore, this variation cannot be explained by Fresnel reflection only but by other effects. As mentioned earlier, the parabolic mirror features imperfections in the form of surface roughness. The variation of the efficiency might follow from scattering at the parabolic mirror and therefore a reduced reference beam quality. Future investigations should use a parabolic mirror of higher quality. Contrary, in the case without beam ratio correction, there is a constant decrease of the efficiencies with increased reference beam angle. Furthermore, there are higher efficiencies for small angles θ. This corresponds to the quality of the employed parabolic mirror. While satisfactory imaging quality can be achieved for small angles, it diminishes noticeably at greater angles. Consequently, other effects than Fresnel reflection must be considered for further investigations. In addition to the quality of the parabolic mirror, non-paraxial reference beam angles impede the overlap of the object and reference beams.

4.2 Holographic Collimator

To enable vHOEs shaping light distributions from a non-collimated LED, the description and synthesis of the wavefront are crucial. The ability to collimate an LED is used as an indicator for the precision of the wavefront approximation. For this purpose, a test setup is built up similar to the sketch in Fig. 1. It uses a phosphor converted white light LED that is placed with a distance of 55 mm and an angle of 50 deg to a vHOE. For comparison, two different vHOEs are exposed with a laser wavelength of 640 nm and an exposure time of 1.2 s. The respective vHOEs consist of 24×24 subholograms on a 20 mm $\times$ 20 mm substrate. The object wave for each subhologram is a plane wave and the reference wave is adapted to the respective angle of incidence.

The first vHOE uses the global angle of incidence adaptation described by Giehl et al.[9] The second vHOE uses the global angle of incidence adaptation in combination with the local wavefront approximation like described in Sec. 2.1. Hereby, the local spherical approximation is realized by displaying phase distributions of spherical lenses on the reference beam SLM. The focal lengths $f_{\mathrm{Ref},i,j}$ of these phase lenses are determined by the distance $d_{i,j}$ of the respective subhologram to the LED. Since a $4f$ system with a beam diameter reduction of the factor 10 is used in the hologram printer, the focal length is given by $f_{\mathrm{Ref}f,i,j} = 10 \cdot d_{i,j}$. The results are shown in Figs. 9 and 10.

A luminance measurement camera (LMK5 Color, TechnoTeam GmbH) with a 50 mm objective lens is used to record luminance distributions of the vHOEs. In the luminance measurements of the vHOEs surfaces shown in Figs. 9(a) and 9(b), the respective subholograms are distinguishable. In the case without local wavefront approximation [see Fig. 9(b)], the subholograms feature

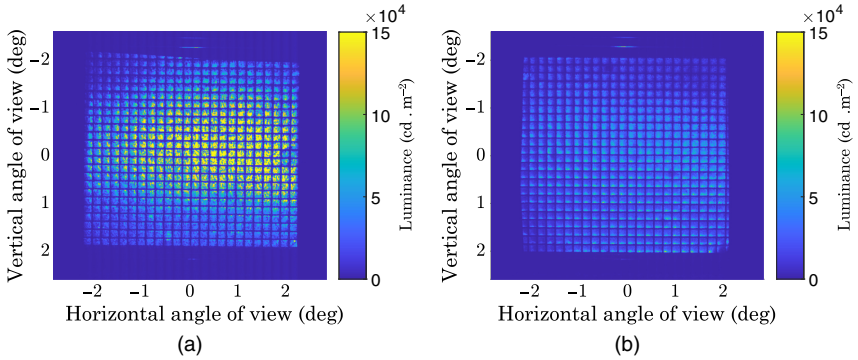

Fig. 9 Luminance measurements of the collimation vHOEs showing the view onto the holograms. (a) Luminance measurement of vHOE with global angle of incidence adaptation only. (b) Luminance measurement of vHOE with global angle of incidence adaptation and local wavefront approximation.

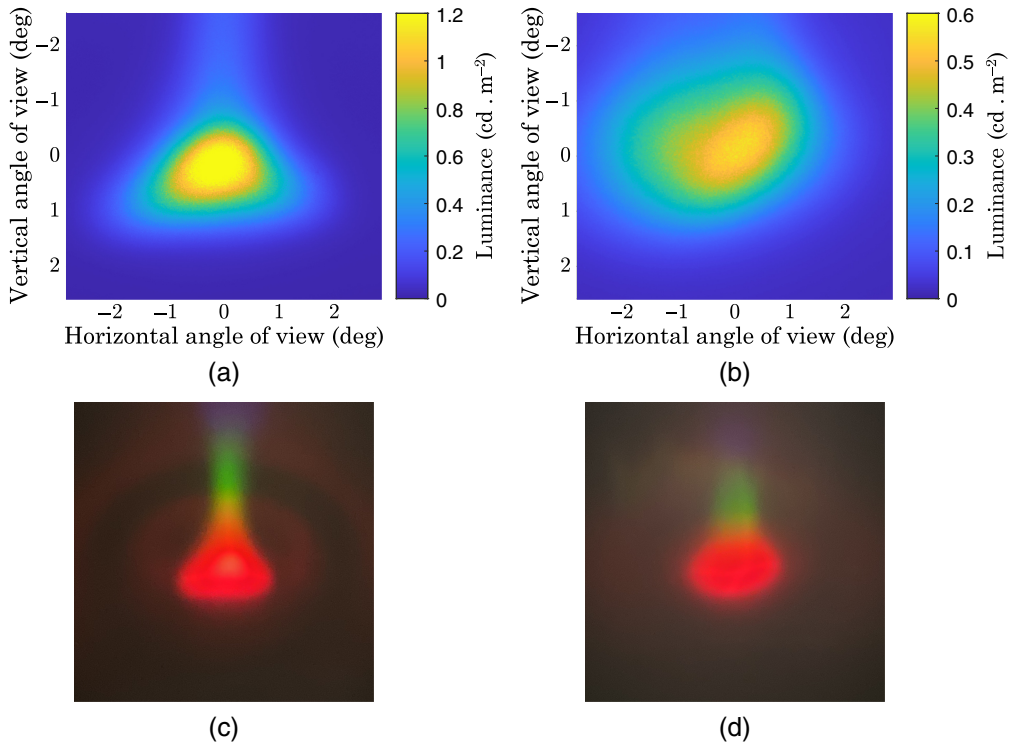

Fig. 10 Luminance measurements and color images of the collimation vHOEs on a screen in a distance of $l = 3$ m. Luminance measurement on screen of the collimation without (a) and with (b) local wavefront approximation. Color image on screen of the collimation without (c) and with (d) local wavefront approximation.

a higher variance of luminance levels with higher luminances in the center of the vHOE. Contrary, in the case with local wavefront approximation [see Fig. 9(b)], the luminance of the subholograms only varies slightly and each subhologram features a bright spot. Without the local wavefront approximation, the vHOE works as an off-axis lens focusing onto the LED chip as a whole. With the local approximation, each subhologram works as an off-axis lens focusing onto the LED chip similar to a micro lens array. Furthermore, the subholograms in Fig. 9(a) show imperfections. Here, the surface quality of the parabolic mirror causes defects. Only a small area of the mirror is used, when the reference beam is a plane wave. Therefore, the surface roughness of the mirror has a big influence. However, in Fig. 9(b), these defects are not present. When adding a spherical wavefront to the reference beam, a larger area of the parabolic mirror is used and the roughness has a smaller influence resulting in a homogeneous appearance of the subholograms. While the beam diameter is larger in the reference beam path due to the concave phase lens on the SLM, the subhologram size keeps the same size in the substrate plane.

The light distributions generated by the vHOEs are shown in Fig. 10. The screen is placed in a distance of $l = 3$ m. The LMK is placed on top of the vHOE. Since the size of the vHOE $h = 20$ mm $\ll l$ and the opening angle from the 50 mm objective lens is known, the divergence can be determined from the luminance measurements. In Fig. 10(a), without the local approximation, the horizontal divergence is full width half maximum $(\mathrm{FWHM}_w) = 1.51$ deg and the vertical divergence is $\mathrm{FWHM}_h = 1.34$ deg. In Fig. 10(b), with the local approximation, the horizontal divergence is $\mathrm{FWHM}_w = 3.32$ deg and the vertical divergence is $\mathrm{FWHM}_h = 2.43$ deg. It was expected that the vHOE with the local wavefront approximation would deliver a better collimation compared to the case without wavefront approximation. However, the results show that the case without local wavefront approximation in Fig. 10(a) provides a better collimation. Furthermore, the shape of the light distributions differs. While the local wavefront approximation vHOE generates a round shaped light distribution and minimal color fringes as shown in Fig. 10(d), the other vHOE generates a triangular shaped light distribution with color fringes in the vertical direction as shown in Fig. 10(c).

It must be noted that these results are only valid for this specific case. The degree of collimation depends on several properties of the setup, the used wavelength, and recording material. The distance of the LED to the vHOE has a large impact. When moving closer to the LED, the local wavefront approximation might be beneficial. Using a longer recording wavelength, like in this case $\lambda = 640$ nm, delivers lower wavelength selectivity compared to shorter wavelengths as shown in Fig. 2. This might explain the color fringes in the case without the local approximation. With the local wavefront approximation, the color fringes are of lower luminance. This and the round shape of the light distribution are good results. The higher divergence might result from the local spherical approximation because using the distance of the LED to the vHOE as a focal length of a spherical lens is an oversimplification. Here, optimization steps must be investigated that take the imaging system of the reference beam and shrinkage of the recording material into account. Future investigations should use a recording material with higher refractive index modulation, a shorter distance between LED and vHOE and an improved calculation of the required spherical approximation.

4.3 Stoplight Function

Finally, the generation of automotive light distributions must be investigated. Due to the lack of diffraction efficiency of the blue (457 nm) vHOEs in Fig. 7(a), only monochromatic light distributions are considered in a first step. A promising use case is a red stoplight function for rear combination lamps. For this investigation, a miniaturized light distribution with limited opening angle is used. The limitation follows from the object SLM and the aperture of beam path as well as the aberrations of the lenses of the $4f$ system.

Currently, stoplights are realized by either using scattering light guides or free-form reflectors. Those free-form reflectors can be converted into phase distributions as described in Ref. 18. The phase distribution is shown in Fig. 11(a). Using the Fraunhofer propagator, the far field light distribution of the stoplight is recovered in Fig. 11(b).

The recovered light distribution in Fig. 11(b) shows a dot pattern with higher intensity in the center and a rectangular shape. However, this light distribution is only expected with laser reconstruction. Using an LED, the light distribution will be blurred, which is beneficial for the use case as a stoplight.

For the experimental investigation of the stoplight function, the test setup with a phosphor converted white light LED of Sec. 4.2 is used. Obviously, in an RCL a red LED should be used in terms of efficiency and regulations. However, due to the wavelength selectivity, the white LED can be used for a first investigation. Again, the vHOE consists of 24×24 subholograms on a 20 mm $\times$ 20 mm substrate and is laminated onto a planar transparent carrier. For exposure, the red ($\lambda = 640$ nm) laser and an exposure time of $t_{\text{exp}} = 1.2$ s is used. Both global angle of incidence adaptation and local wavefront approximation are applied. The results are shown in Fig. 12.

Figure 12 shows luminance measurements of the vHOE [Fig. 12(a)] and of the projected light distribution [Fig. 12(b)]. The vHOE appears homogeneous and the light distribution is square with higher intensity toward the center. The opening angle of the light distribution is $\approx \pm 3$ deg horizontally and $\approx \pm 2$ deg vertically, which matches the expectations. However,

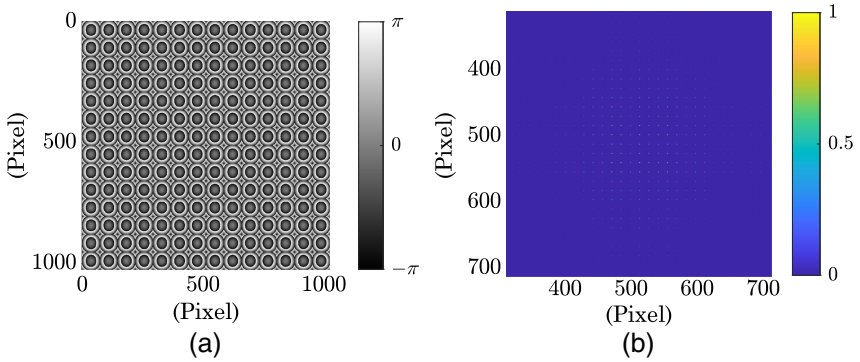

Fig. 11 Scaled stoplight distribution. (a) Phase distribution for a scaled stoplight distribution for $\lambda = 640$ nm. (b) Fraunhofer simulation of far field light distribution of the phase distribution.

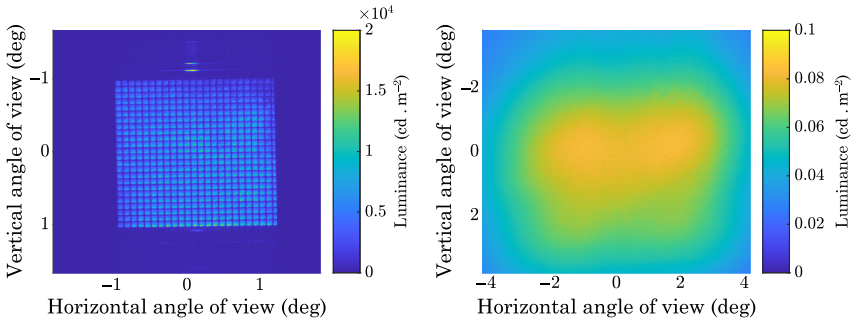

Fig. 12 Luminance measurements of the stoplight. (a) Luminance measurement of the stoplight vHOE. (b) Luminance measurement of the stoplight distribution on a screen.

the center features two local bright spots instead of a single one. This might follow from shrinkage of the foil after exposure and consequently aberrations. Furthermore, the achieved luminances are very low and far from the legal requirements. The low luminance of the light distribution follows from the large distance of the LED to the vHOE. Most of the light is lost due to divergence of the LED. In the used test setup, there is no possibility to reduce the distance of LED and vHOE. Future test setups should feature an improved positioning of the LED and vHOE. A primary collimation of the LED is also possible but is not the scope of this investigation.

Nevertheless, the results prove the concept of a holographic stop light function in a miniaturized version. With red high power LEDs, larger and segmented vHOEs, and a closer distance to the LEDs, a stop light function fulfilling the legal requirements should be possible.

5 Summary

In this paper, an advanced printer for vHOEs is presented. The aim is to manufacture vHOEs for automotive exterior lighting that can be reconstructed with an LED and generate a specific light distribution. The presented printer features four laser wavelengths, two phase only SLMs, and a complex optical system to vary the incidence angle of the reference beam during exposure over a large angular range. The LED's wavefront should be approximated with a combination of the global angle of incidence adaptation using a parabolic mirror and the local spherical wavefront approximation using the reference beam SLM. Several optical path lengths, polarizations, and beam ratio adaptations are required and implemented. First investigations show good results for the diffraction efficiency of simple slanted gratings for 532, 594, and 640 nm with $\eta > 40\%$. For 457 nm, however, only low diffraction efficiencies $\eta < 20\%$ are achieved. In addition, the diffraction efficiency for different reference beam angles was investigated to validate the implemented beam correction mechanisms. Although performing better than without the beam ratio correction, there is still a large variation in the diffraction efficiency for the different reference beam angles. This implies that it is not sufficient to compensating the Fresnel reflection and optical path length only but an additional characterization of the setup is required. Particularly, the parabolic mirror features imperfections reducing the imaging quality of the reference beam strongly. Here, a new or refurbished mirror might be the solution for better predictability of the results. An indicator for the accuracy of the wavefront approximation of the LED is given by the ability of the vHOE to collimate the LED light. Two approaches for collimating an LED with a vHOE were investigated. Good collimation was achieved for both cases using the global angle of incidence adaptation only ($\mathrm{FWHM}_w = 1.51$ deg, $\mathrm{FWHM}_h = 1.34$ deg) and with additional local wavefront approximation ($\mathrm{FWHM}_w = 3.32$ deg, $\mathrm{FWHM}_h = 2.43$ deg). While the case without local wavefront approximation delivers a better collimation, it features color fringes and geometrical aberrations. With the local wavefront approximation, color fringes could be reduced and the light distribution has a nearly circular shape. Finally, first investigations to generate an automotive light distribution with a vHOE showed promising results. Although only showing a miniaturized stoplight function with low output, it was shown that projecting light distributions with a vHOE and LED illumination is possible.

For all exposures, the standard BAYFOL HX 200 material was used. Future investigations should feature a material with higher refractive index modulation capability. Until now only monochromatic vHOEs were tested. Once the exposure parameters are optimized, sequential exposure of all four wavelengths will be used to generate white light distributions. Further improvement of the wavefront approximation and the printer setup could enable a sharp lensless projection of a low beam distribution providing white color and high contrast at the cutoff. Different algorithms for CGH will be benchmarked regarding their suitability for LED reconstruction.

Code and Data Availability

The code that supports the findings of this paper is not publicly available because it is property of HELLA GmbH & Co. KGaA, Rixbecker Straße, 59552 Lippstadt, Germany. The measurement data can be requested from the author at lukas.hiller@l-lab.de.

Acknowledgments

This paper is based on the SPIE Proceedings Paper 12910-24 with the title "Advanced printer for volume holographic optical elements in automotive exterior lighting," of the conference *Practical Holography XXXVIII: Displays, Materials, and Applications*. The authors extended this paper with additional results regarding the generation of automotive light distributions with vHOEs and LED illumination.

References

1. D. Gabor, "A new microscopic principle," *Nature* **161**, 777 (1948).
2. E. N. Leith and J. Upatnieks, "Zone plate with aberration correction," *J. Opt. Soc. Am.* **57**, 699 (1967).
3. F.-K. Bruder et al., "Precision holographic optical elements in Bayfol HX photopolymer," *Proc. SPIE* **9771**, 977103 (2016).
4. H. Kogelnik, "Coupled wave theory for thick hologram gratings," *Bell Syst. Tech. J.* **48**, 2909–2947 (1969).
5. D. Karthaus, O. Sandfuchs, and S. Sinzinger, "Transmission volume holograms for LED illumination," in *Ilmenau Scientific Colloquium. Technische Universität Ilmenau*, Vol. 59, ilmedia (2017).
6. D. Karthaus et al., "Modeling of light-emitting diode wavefronts for the optimization of transmission holograms," *Appl. Opt.* **56**, 5234–5241 (2017).
7. D. Karthaus et al., "Optimization of computer-generated transmission holograms using different LED wavefront approximations," in *DGaO-Proc. 2017*, D. G. für angewandte Optik e.V., Ed., Bremen (2017).
8. D. Karthaus, O. Sandfuchs, and S. Sinzinger, "Optimization of holograms for application in automotive headlamps with LED illumination," in *Imaging and Appl. Opt. 2016*, OSA, Washington, D.C., p. 417 (2016).
9. M. Giehl, S. Alt, and C. Neumann, "Adaptation of volume holographic cell arrays to divergent LED illumination," in *DGaO-Proc. 2020*, D. G. für angewandte Optik e.V., Ed., Bremen (2020).
10. F.-K. Bruder et al., "Diffractive optics in large sizes: computer-generated holograms (CGH) based on Bayfol HX photopolymer," *Proc. SPIE* **9385**, 93850C (2015).
11. J. Hofmann et al., "Extended holographic wave front printer setup employing two spatial light modulators," *Proc. SPIE* **11030**, 110300N (2019).
12. M. Giehl, L. T. Hiller, and C. Neumann, "Manufacturing of volume holographic cell arrays for usage with uncollimated LEDs in automotive applications," *Adv. Opt. Technol.* **9**, 349–355 (2020).
13. D. Karthaus, O. Sandfuchs, and S. Sinzinger, "Holograms in automotive headlamps - chances and challenges," in *DGaO-Proc. 2015*, D. G. für angewandte Optik e.V., Ed., Bremen (2015).
14. L. Hiller and J. Wallaschek, *Chromaticity of White Light Volume Holographic Cell Arrays for Divergent Illumination with Phosphor Converted LEDs in Automotive Headlights*, TU Ilmenau (2021).
15. Wirtschaftskommision der Vereinten Nationen für Europa, "Regelung nr. 112 der Wirtschaftskommission für Europa der Vereinten Nationen (unece) - Einheitliche Bedingungen für die Genehmigung der Kraftfahrzeugscheinwerfer für asymmetrisches Abblendlicht und/oder Fernlicht, die mit Glühlampen und/oder Led-Modulen ausgerüstet sind," *Amtsblatt Eur. Union* **L 250**, 67–128 (2014).
16. R. W. Gerchberg and W. O. Saxton, "A practical algorithm for the determination of phase from image and diffraction plane pictures," *Optik* **35**, 237–246 (1972).
17. F. Wyrowski and O. Bryngdahl, "Iterative Fourier-transform algorithm applied to computer holography," *J. Opt. Soc. Am. A* **5**, 1058 (1988).
18. L. T. Hiller and J. Wallaschek, "Converting automotive free-form reflectors into phase images for computer-generated holograms," in *Digital Hologr. and 3-D Imaging 2022*, Optica Publishing Group, Washington, D.C., p. **34** (2022).

19. K. Hens et al., "Lasers for holographic applications: important performance parameters and relevant laser technologies," *Proc. SPIE* **10944**, 1094408 (2019).
20. B. E. A. Saleh and M. C. Teich, *Grundlagen der Photonik, Lehrbuch Physik*, 1st ed., Wiley-VCH Verlag GmbH & Co. KGaA, Weinheim, [deutsche Übersetzung von] 2., vollständig überarbeitete und erweiterte auflage [des werkes] ed. (2008).
21. H. Berneth et al., "Holographic recordings with high beam ratios on improved Bayfol® HX photopolymer," *Proc. SPIE* **8776**, 877603 (2013).
22. H. Berneth et al., "Holographic recording aspects of high-resolution Bayfol HX photopolymer," *Proc. SPIE* **7957**, 79570H (2011).

Lukas T. Hiller received his BSc degree in physics in October 2018 and his MSc degree in optical technologies in December 2020 from Leibniz University in Hanover. He started his PhD at the L-LAB, HELLA's unique international research institute for automotive lighting and mechatronics. During his bachelor thesis, he worked on the manufacturing of diffractive optical elements at the Hanover Centre for Optical Technologies. In his masters, he started his work at the L-LAB focusing on the improvement of a hologram printer for volume holographic optical elements (vHOEs) and the concept of a hologram-based automotive headlamp. Continuing with his PhD, he works on hologram-based automotive lighting. The work addresses vHOEs for white light distributions and LED reconstruction, algorithms for the calculation of computer generated holograms, new automotive lighting concepts, and the improvement of the hologram printer.

Jörg Wallaschek is director of the Institute of Dynamics and Vibration Research at Leibniz Universität Hannover. His research is focused on applied dynamics, piezoelectric and ultrasonic engineering as well as automotive lighting. He is a member of the Scientific Advisory Board of L-LAB and works closely with industry, including as a member of the Innovation Boards of various companies. He has authored more than 200 scientific publications and patent applications.